# Investigation on coupling effects between surface wear and dynamics in a spur gear system

Xianzeng Liu, Yuhu Yang, Jun Zhang

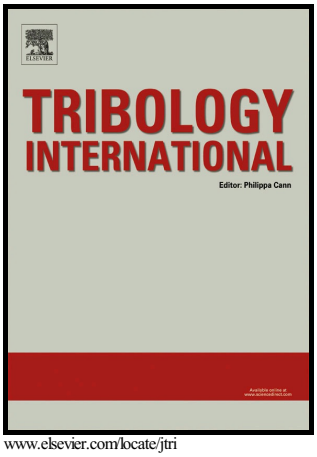


www.elsevier.com/locate/jtri

PII: S0301-679X(16)30097-4
DOI: http://dx.doi.org/10.1016/j.triboint.2016.05.006
Reference: JTRI4185

To appear in: *Tribiology International*

Received date: 19 March 2016
Revised date: 3 May 2016
Accepted date: 5 May 2016

Cite this article as: Xianzeng Liu, Yuhu Yang and Jun Zhang, Investigation or coupling effects between surface wear and dynamics in a spur gear system *Tribiology International,* http://dx.doi.org/10.1016/j.triboint.2016.05.006

# Investigation on Coupling Effects between Surface Wear and Dynamics in a Spur Gear System

Xianzeng Liu [a], Yuhu Yang [a], Jun Zhang [b,*]

[a] School of Mechanical Engineering, Tianjin University, Tianjin, 300072, P. R. China

[b] School of Mechanical Engineering and Automation, Fuzhou University, Fuzhou, 350116, P. R. China

*Corresponding author. E-mail: zhang_jun@tju.edu.cn

**Abstract:** A dynamic wear prediction methodology is proposed to investigate the coupling effects between surface wear and dynamics of spur gear systems. The overall computational scheme combines a quasi-static wear model and a translational-rotational-coupled nonlinear dynamic model. The worn surfaces are represented by modulated mesh excitations and introduced into the dynamic model to investigate the effects of surface wear on system's dynamic characteristics. The dynamic gear mesh forces are converted into an equivalent load by using the Miner rule to reveal the effects of dynamics on wear behaviors. A spur gear transmission is taken as an example system to demonstrate the interactions between surface wear and dynamic behaviors. The simulations indicate that surface wear and gear dynamics are highly interacted.

**Keywords:** gear dynamics; gear wear; mesh stiffness; transmission error

## 1. Introduction

Gear systems are widely used in various power transmission applications due to their distinguished merits of accurate transmission ratio, large power range, high transmission efficiency and stable operation quality. For a gear system worked in dirty envirioments with heavy duties, the surface wear and the vibration are considered two major causes of operational failure. To improve the transmission accuracy and avoid premature fatigue, numerous efforts have been carried out to investigate the vibration mechanism of gear systems [1-7] and the wear mechanism of gear teeth [8-32].

As addressed in previous studies, surface wear and gear vibration are mutually affected by each other [8-17]. As a long-term material removal behaviour, surface wear results in a deviation from the intended tooth profile and alters the gear mesh excitations, which makes the dynamic behaviors of a gear system with worn surfaces quite different from their counterparts without wear. Surface wear not only alters the stress and load distributions but also aggravates system's characteristics of vibration and noise. On the other hand, the dynamic loads caused by system vibration are different from

| | | | |
|---|---|---|---|
| $A_e$, $B_e$ | Magnitudes of AM and FM for STE | $m_p$, $m_g$ | Mass of pinion and gear |
| $A_k$, $B_k$ | Magnitudes of AM and FM for mesh stiffness | $n$ | Number of harmonic terms |
| $F_{aT}$ | Fluctuating force | $n_1$ | Speed of pinion |
| $F_{aTr}$ | Harmonic amplitude of fluctuating force | $p$ | Contact pressure |
| $F_m$ | Average mesh force | $q$ | Number of pressure update |
| $F_p$, $F_g$ | External radial preloads of bearings | $s$ | Sliding distance |
| $I_p$, $I_g$ | Mass moments of inertia for pinion and gear | $t$ | Time |
| $R_p$, $R_g$ | Radii of base circles for pinion and gear | $u$ | Relative displacement along the line of action |
| $T_{eq}$ | Equivalent load | $y_p$, $y_g$ | Transverse displacements of pinion and gear |
| $T_j$ | Torque at each discrete time instant | $\delta$ | Displacement in the direction of the path of action |
| $T_p$, $T_g$ | Input torque and output torque | $\delta_{H1,2}$ | Hertz flattening |
| $2b$ | Backlash value of gear pair | $\delta_{RK}$ | Gear body deformation |
| $c_m$ | Mesh damping | $\delta_Z$ | Gear tooth bending |
| $c_{py}$, $c_{gy}$ | Damping of bearings for pinion and gear | $\varepsilon^q$ | Predetermined wear threshold |
| $e$ | STE | $\varepsilon^t$ | Maximum allowable wear threshold |
| $e_r$ | $R$-th harmonic amplitudes for STE | $\zeta$ | Number of wear cycles |
| $h$ | Wear depth | $\theta_p$, $\theta_g$ | Torsional displacements of pinion and gear |
| $k$ | Wear coefficient | $\varphi_{aTr}$ | Harmonic phase angle input torque excitation |
| $k_{ar}$ | $R$-th harmonic amplitudes for mesh stiffness | $\varphi_{ea}$, $\varphi_{eb}$ | Initial phases of AM and FM for STE |
| $k_m$ | Time-varying stiffness | $\varphi_{er}$ | Harmonic phase angles of STE |
| $k_{mm}$ | Average mesh stiffness | $\varphi_{ka}$, $\varphi_{kb}$ | Initial phases of AM and FM for mesh stiffness |
| $k_{t1,t2}$ | Total stiffness of one tooth pair | $\varphi_{mr}$ | Harmonic phase angle of mesh stiffness |
| $k_{p,g}$ | Individual stiffness of one tooth | $\omega_{aT}$ | Fundamental frequency of input excitation |
| $k_{py}$, $k_{gy}$ | Bearing stiffness of pinion and gear | $\omega_e$ | Fundamental frequency of STE |
| $l$ | Slope of the Wöhler-damage line | $\omega_m$ | Fundamental frequency of mesh stiffness |
| $m_c$ | Equivalent mass of gear pair | | |

the static loads, which increases the contact pressures between the mating surfaces and fasten the wear process. From this point of view, the gear system dynamics also affects the surface wear characteristics significantly.

Although the investigations on surface wear and gear dynamics are abundant, the studies focused on the their coupling effects are quite few. Among these few studies, most of the them are concentrated on the effects of surface wear on the dynamics of a gear system [8-14]. For example, Choy et al. [8] studied how the surface pitting and wear affect the vibrations of a gear system. The effect of surface wear was represented by the change of gear mesh stiffness which was then introduced into a gear-shaft model. Wojnarowski and Onishchenko [9] established a two degrees-of-freedom elastic dynamic model with worn teeth to study the impacts of surface wear on spur gear dynamics. Yesilyurt et al. [10] investigated the influence of surface wear on the change of gear mesh stiffness from the durability and diagnostic points of view. Their study manifested that the effect of surface wear on the system's dynamics was primarily caused by the

deviations in tooth shape from the idea involute profile. Kuang and Lin [11] investigated the effect of surface wear on the variation of vibration spectrum of a spur gear system by combining a single degree-of-freedom dynamic model with a wear prediction model developed by Flodin et al. [18,19]. The simulation results showed that the surface wear may change the dynamic load histogram of an engaging spur gear pair greatly. Later, they carried out a similar investigation for an engaged plastic gear pair [12]. However, in their studies only the dynamics at one rotational speed were investigated. Yuksel and Kahraman [13] combined a wear prediction model proposed by Bajpai et al. [23] and a deformable-body dynamic model [33] to study the influence of quasi-static wear profiles on the dynamics of a planetary gear set. The worn surfaces were introduced into the dynamic model to quantify the effect of surface wear on the dynamic gear meshing forces. Nevertheless, the surface wear behaviors under dynamic conditions were not discussed in this study. Osman and Velex [14] combined a dynamic model with a wear model based on Archard's law to investigate the effect of surface wear on the dynamic responses of a wide-faced gear.

Compared with the studies of the effects of surface wear on gear dynamics, the investigationes on the effect of gear dynamics on the surface wear behaviors were even less [16,17]. Ding and Kahraman [16] combined a one degree-of-freedom dynamic model with Bajpai's wear prediction model [23] to study the interactions between the surface wear and the dynamics in a spur gear system. In this study, the effects of wear profiles were represented by a periodically time-varying mesh stiffness function and an external displacement excitation. More recently, they extended the methodology to a planetary gear system to investigate the interactions between the surface wear and the system's dynamic behaviors [17].

From the above reviews, it can be found that there is common thread in the efforts of investigating the coupling effects between the surface wear and gear dynamics in that the worn surfaces are treated as internal excitations (time-varying meshing stiffness and/or transmission error) incorporated with certain kind of dynamic model of a gear system. Based on these dynamic models, the effects of surface wear on the dynamic behaviors of gear are investigated and vice versa. However, it needs to point out that an accurate prediction for the gear dynamics relies on a comprehensive dynamic model. Unfortunetly, the dynamic models used in the above studies only included the torsional

deflections in gear-shaft systems. The translational effects coming from the shaft bending and bearing radial deflections were not considered in these dynamic models, which may degenerate the prediction accuracy of the dynamic analysis. To guarantee the prediction accuracy, a comprehensive translational-rotational-coupled nonlinear dynamic model with three degree-of-freedom for a spur gear system is proposed and then combined with a quasi-static wear model proposed earlier by the authors [32]. Based on this combined dynamic surface wear prediction methodology, the effects of surface wear on the dynamic behaviors of the spur gear system are investigated. Meanwhile, the influences of the dynamic loads on the surface wear behaviors are studied by converting the steady-state dynamic gear forces into an equivalent load with the Miner rule. The converted equivalent load is introduced into the quasi-static wear model to reveal the surface wear process under dynamic load conditions.

A thorough understanding of the coupling effects between the gear wear and the gear dynamics helps to prolong the service life and improve the performance of gear sets. Motivated by this thought, the main contents of this paper are arranged as the follows. In section 2, a translational-rotational-coupled nonlinear dynamic model for a spur gear system is developed which incorporates the effect of worn surfaces of the mating gear pair. The profile deviations from surface wear are represented in the forms of gear mesh excitation and transmission error functions with amplitude and frequency modulations. In section 3, a dynamic wear prediction methodology is proposed by combining the proposed dynamic model with the aforementioned quasi-static wear model [32]. In section 4, a spur gear system is taken as an example to demonstrate the coupling effects between the surface wear and the dynamic responses. Finally, some conclusions are drawn in section 5.



## 2. Dynamic modeling for a spur gear system

In this section, an analytical nonlinear dynamic model for a spur gear system with surface wear is established, with which the dynamic behaviors of the system can be predicted.

By simplifying the real-world gear system into a mass-spring-damping system, a lumped parameter nonlinear dynamic model for a spur gear system developed by Kahraman and Singh [2] can be illustrated as shown in Fig. 1.

Herein, $I_p$ and $I_g$ denote the inertias of the pinion and the gear, respectively. Similarly, the mass of the pinion and that of the gear are represented with $m_p$ and $m_g$, respectively. $R_p$ and $R_g$ illustrate the base circles of the pinion and the gear. Assume that $\theta_p, \theta_g$ and $y_p, y_g$ are the torsional and the transversal displacements of the pinion and the gear while $F_p$ and $F_g$ are the external radial preloads applied to the rolling element bearings. The gear mesh is described by a nonlinear displacement function $f(u)$ with time-varying stiffness $k_m(t)$ and viscous damping $c_m$. Meanwhile, a static transmission error (STE) of the gear pair is introduced and represented as $e(t)$. The radial stiffness and damping effects of rolling element bearings are marked as $k_{py}$, $k_{gy}$ and $c_{py}$, $c_{gy}$, respectively. $T_p(t) = T_{pm} + T_{pa}(t)$ and $T_g(t) = T_{gm} + T_{ga}(t)$ are the external torques acting on the pinion and the gear, with $T_{pm}/T_{gm}$ and $T_{pa}(t)/T_{ga}(t)$ being the constant part and the fluctuation part respectively.

As demonstrated in Fig. 1, the proposed lumped parameter dynamic model considers both the torsional and the transversal deflections in the spur gear system and the damping effects as well. By using the 2nd Newtonian law, the following equations of motion can be formulated.

$$\left.\begin{aligned} &m_p\ddot{y}_p + c_{py}\dot{y}_p + k_{py}y_p + k_m(t)f(u) + c_m\dot{u} = -F_p \\ &m_g\ddot{y}_g + c_{gy}\dot{y}_g + k_{gy}y_g - k_m(t)f(u) - c_m\dot{u} = F_g \\ &m_c\left(\ddot{u} - \ddot{y}_p + \ddot{y}_g\right) + k_m(t)f(u) + c_m\dot{u} = F_m + F_{aT}(t) - m_c\ddot{e}(t) \end{aligned}\right\} \tag{1}$$

Herein, an over dot denotes differentiation with respect to time $t$. $u$ is the relative displacement along the line of action, $m_c$ is the equivalent mass of the gear pair; $F_m$ is the average mesh force, $F_{aT}(t)$ is the fluctuating force related to the external input torque excitation. These variables can be further expressed as the followings.

$$u = R_p\theta_p - R_g\theta_g - e + y_p - y_g \tag{2}$$

$$m_c = I_pI_g\big/\left(I_gR_p^2 + I_pR_g^2\right) \tag{3}$$

$$F_m = T_{pm}/R_p = T_{gm}/R_g \tag{4}$$

$$F_{aT}(t) = m_cR_pT_{pa}(t)/I_p \tag{5}$$

The nonlinear displacement function $f(u)$ can be described as the following

$$f(u) = \begin{cases} u - b, & u > b \\ 0, & -b \le u \le b \\ u + b, & u < -b \end{cases} \tag{6}$$

where 2*b* is the backlash value of the gear pair.

The periodic time-varying stiffness $k_m(t)$ can be given by [2]

$$k_m(t) = k_{mm} + \sum_{r=1}^{n} k_{ar} \cos(r\omega_m t + \varphi_{mr}) \tag{7}$$

where $k_{mm}$ is the mean component of $k_m(t)$, $k_{ar}$ is the amplitude of the *r*-th harmonic mesh stiffness content, $\varphi_{mr}$ is the corresponding phase angle of the *r*-th harmonic mesh stiffness, *n* is the number of harmonic terms sufficient to describe the periodic function, $\omega_m$ is the fundamental frequency of the mesh stiffness.

Similarly, the static transmission error $e(t)$ can be expressed as

$$e(t) = \sum_{r=1}^{n} e_r \cos(r\omega_e t + \varphi_{er}) \tag{8}$$

where $e_r$ is the amplitude of the *r*-th harmonic static transmission error, $\varphi_{er}$ is the phase angle of the *r*-th harmonic static transmission error and $\omega_e$ is the fundamental frequency of static transmission error.

$F_{aT}(t)$ is assumed to include the same harmonics as $k_m(t)$ and $e(t)$ which can be formulated as

$$F_{aT}(t) = \sum_{r=1}^{n} F_{aTr} \cos(r\omega_{aT} t + \varphi_{aTr}) \tag{9}$$

where $F_{aTr}$ is the amplitude of the *r*-th harmonic fluctuating force, $\varphi_{aTr}$ is the phase angle of the *r*-th harmonic content and $\omega_{aT}$ is the fundamental frequency of input torque excitation .

The worn surfaces of gears can be regarded as faults deviating from the perfect gear surfaces, which in turn, will produce amplitude modulation (AM) and frequency modulation (FM) effects on gear mesh vibrations [34]. From this point of view, the mesh excitations arousing from a gear pair with distributed worn surfaces can be modeled by amplitude and frequency modulations process [35]. For simplicity, only the fundamental harmonic of $k_m(t)$ and $e(t)$ are considered in this paper though the higher harmonics can be easily included. After considering the fundamental harmonic effect of surface wear the gear pair, one can formulate the mesh stiffness function with amplitude and frequency modulations as

$$k_m(t) = k_{mm} + a_k(t) k_{a1} \cos(\omega_m t + \varphi_{m1} + b_k(t)) \tag{10}$$

$$a_k(t) = 1 + A_k \cos(\omega_m t + \varphi_{ka}), \quad b_k(t) = B_k \sin(\omega_m t + \varphi_{kb}) \tag{11}$$

where $A_k$ and $B_k$ are the amplitudes of AM and FM, respectively; $\varphi_{ka}$ and $\varphi_{kb}$ are the initial phases of AM and FM, respectively.

Similarly, the static transmission error excitation with worn surfaces effects can be rewritten as the following

$$e(t) = a_e(t) e_1 \cos\left(\omega_e t + \varphi_{e1} + b_e(t)\right) \tag{12}$$

$$a_e(t) = 1 + A_e \cos\left(\omega_e t + \varphi_{ea}\right), \quad b_e(t) = B_e \sin\left(\omega_e t + \varphi_{eb}\right) \tag{13}$$

where $A_e$ and $B_e$ are the amplitudes of AM and FM, respectively; $\varphi_{ea}$ and $\varphi_{eb}$ are the initial phases of AM and FM, respectively.

The above modulation parameters can be pre-determined through loaded tooth contact analysis (LTCA) [32]. To ensure maximum portability and reusability, the LTCA was performed by using the commercial software Kisssoft®. In the LTCA, the gear tooth bending $\delta_{Zi}$, the body deformation $\delta_{RKi}$ and the Hertz flattening $\delta_{H1,2}$ of an individual gear are taken into account ($i=p, g$) [36]. Therefore, the displacement of an individual gear along of the line of action can be summarized as

$$\delta_i = \delta_{Zi} + \delta_{RKi} + \delta_{H1,2} \tag{14}$$

The stiffness of one single tooth of an individual gear can be obtained as

$$k_i = \frac{F_i}{\delta_i} \tag{15}$$

Hence, the total stiffness of one tooth pair could be calculated as the following

$$k_{t1} = \frac{k_p + k_g}{k_p k_g} \tag{16}$$

In cases where there are two pairs in contact, the stiffness $k_{t2}$ for the second tooth pair can be obtained with the same procedure. Then the equivalent mesh stiffness can be summarized as the follow

$$k_m = k_{t1} + k_{t2} \tag{17}$$

Accordingly, the static transmission error can be expressed as

$$e = \delta_p + \delta_g \tag{18}$$

The above procedure for determining the mesh stiffness and the static transmission error can be applied to a gear pair with and without worn surfaces.

After introducing the modulated excitations defined by Eq. (10) and (12) into Eq. (1), the nonlinear differential

equation of motion of the spur gear system can be solved by employing a fourth-order variable-step Runge-Kutta numerical integration method. With MATLAB coding, the dynamic behaviors such as steady-state dynamic responses of a spur gear system with worn surfaces can be determined, which is then integrated with the following quasi-static wear model to predict the dynamic wear of the gear system.

## 3. Dynamic wear prediction methodology for a spur gear system

In this section, a dynamic wear prediction methodology for spur gear system is presented by combining the aforementioned nonlinear dynamic model with a quasi-static wear model previously proposed by the authors [32]. For the convenience of understanding, the establishment of a quasi-static wear model for a spur gear system is briefly introduced though the details can be referred to our previous publication [32].

### *3.1. Quasi-static wear model for a spur gear system*

The authors developed a quasi-static wear model to predicte the surface wear of spur gears under static load conditions. The basic idea of this model is to employ Archard's wear equation to compute the wear depth of a local point on one of the mating surfaces in the integration form of the following

$$h = \int_0^s kpds \tag{19}$$

where $h$ is the wear depth, $s$ is the sliding distance, $p$ is the contact pressure and $k$ is the wear coefficient.

Fig. 2 shows the flowchart of the overall wear prediction model.

As shown in Fig. 2, a three dimensional (3D) finite element (FE) model is developed to compute the mean value of contact pressures of meshed grids on the mating surfaces, which is then combined with the sliding distance and the wear coefficient to calculate the wear depth. Once the wear depth of any point on mating surfaces during one wear cycle is obtained, the above integral process is repeated until the wear depth of any point on the contact surfaces reaches a predetermined wear threshold, under which the contact pressures change accordingly. Then the gear surface needs to be reconstituted to perform another contact analysis for renewed surface pressures. The iterative process is repeated until the

maximum total wear depth on either of the two gears reaches a maximum allowable wear threshold. The wear depth of every point on the surface is obtained by summing up wear depths of every point accumulated in all processes of different pressure updates.

To be more specific, the wear depth occurrs at each node *ij* of the fixed surface grid during one wear cycle can be calculated through Eq. (19) with calculated *k*, *p* and *s*. If the wear depth of any node on the contact surfaces reaches the predetermined wear threshold $\varepsilon^q$ after the *q*-th pressure update, the geometry of gear surface needs to be reconstituted to perform contact analysis afresh for renewed surface pressure. The iterative process is repeated until the maximum total wear depth on either of the two gears reaches the maximum allowable wear threshold $\varepsilon^t$.

The accumulated wear depth at any node *ij* during one wear cycle is given as

$$\left(\Delta h_{ij}^q\right)_\zeta^{p,g} = k\left(\bar{p}_{ij}^q\right)_\zeta^{p,g}\left(s_{ij}^q\right)_\zeta^{p,g} \tag{20}$$

where $\left(\bar{p}_{ij}^q\right)_\zeta^{p,g}$ is the mean pressure value at node *ij* during one wear cycle, and $\left(s_{ij}^q\right)_\zeta^{p,g}$ is the sliding distance at node *ij* during one wear cycle after the *q*-th pressure update.

Eq. (20) is applied continuously $\zeta^q$ times until the wear depth accumulated at any node of either one of the contacting surfaces after the *q*-th geometry update reaches the threshhold of $\varepsilon^q$. Then, the wear amounts at nodes *ij* accumulated since the last geometry update are given as:

$$\left(h_{ij}^q\right)^{p,g} = \zeta^q\left(\Delta h_{ij}^q\right)_\zeta^{p,g} \tag{21}$$

The total number of wear cycles $\zeta^q$ is given as:

$$\zeta^q = \frac{\varepsilon^q}{\max\left\{\left(\Delta h_{ij}^q\right)_\zeta^p, \left(\Delta h_{ij}^q\right)_\zeta^q\right\}} \tag{22}$$

The wear amounts accumulated after each geometry updated are summed to get the final wear depth of node *ij* as:

$$h_{ij}^{p,g} = \sum_{q=1}^{Q}\left(h_{ij}^q\right)^{p,g} \tag{23}$$

The total number of wear cycles required to reach to this wear depth is:

$$\zeta^t = \sum_{q=1}^{Q}\zeta^q \tag{24}$$

### 3.2. *Dynamic wear prediction methodology*

As can be observed from the above descriptions for quasi-static wear modeling, the computation for the surface wear of spur gears uses the mean values of contact pressures instead of dynamic contact loads on the mating surfaces. In a real-world gear system, however, the contact pressures on the mating surfaces are time-varying due to gear mesh excitations. Therefore, to predict the surface wear of a spur gear system under dynamic load conditions, we propose a dynamic wear model by integrating the nonlinear dynamic model with the quasi-static wear model. The computational methodology employed here to predict the dynamic wear of contacting gear surfaces is shown in Fig. 3.

As demonstrated in Fig. 3, an LTCA is performed at the beginning to obtain the static transmission error $e^q(t)$ and the time-varying stiffness $k_m^q(t)$ for each geometry update $q$. $e^q(t)$ and $k_m^q(t)$ are used as excitations for the nonlinear dynamic analysis to predict the steady-state dynamic responses of the gear system at a given rotational speed. As one of the response parameters, the relative displacement along the line of action after the $q$-th geometry update $u^q$ is obtained and the dynamic gear mesh force (DMF) is calculated as $F_m^q(t) = k_m^q(t)\, f\left(u^q(t)\right)$.

Based on the linear cumulative damage rule commonly referred as the Miner rule [37], the equivalent load $T_{eq}^q$ is obtained from for each geometry update $q$ [38]

$$T_{eq}^q = \left( \frac{n_1 \left(T_1^q\right)^l + n_2 \left(T_2^q\right)^l + \ldots + n_j \left(T_j^q\right)^l}{n_1 + n_2 + \ldots + n_j} \right)^{\frac{1}{l}} \tag{25}$$

where $T_j^q$ is the torque at each discrete time instant $t$ from $T_m^q(t)$, $n_j$ is the corresponding times of occurrence of $T_j^q$, $l$ is the slope of the Wöhler-damage line. And $T_m^q(t)$ can be calculated through the following equation

$$T_m^q(t) = R_p F_m^q(t) \tag{26}$$

The equivalent torque $T_{eq}^q$ is input back into the contact model of the gear pair to compute the contact pressure $p$ of engaging surfaces. By integrating the obtained contact pressure with sliding distance $s$ and the wear coefficient $k$ as formulated in Eq. (19), the wear depth of any point on the engaging surfaces can be computeed. Similar to the descriptions for the flowchart demonstrated in Fig. 2, once the wear depth of any point on the contact surfaces reaches the

predetermined wear threshold to warrant a geometry update, the geometry of gear surface needs to be reconstituted to perform contact analysis afresh for renewed $e^q(t)$ and $k_m^q(t)$. The renewed dynamic analysis and contact analysis are utilized to obtain the updated pressures. With the updated pressures, the new wear computations are performed. The iterative process is repeated until the maximum total wear depth on either of the two gears reaches the maximum allowable wear threshold.

This study employs the same approximate method used by Ding and Kahraman [16] to take into account the influence of lubrication conditions at the gear mesh contact on the wear coefficient *k*. They expressed the wear coefficient *k* as

$$k = \begin{cases} k_0, & \lambda < \frac{1}{2} \\ \frac{2}{7}k_0(4-\lambda), & \frac{1}{2} < \lambda < 4 \\ 0, & \lambda > 4 \end{cases} \tag{27}$$

where $k_0$ is the wear coefficient that corresponds to the values observed at relatively low speeds, $\lambda$ is the so-called lambda ratio. The detailed descriptions can be found in the literature [16].

## 4. Numerical Simulation and Discussions

With the dynamic wear prediction methodology proposed in Section 3.2, a numerical example [5] is used to demonstrate the prediction of wear depth of engaging gear surfaces under dynamic condition. Then the coupling effects between the surface wear and the dynamic behaviors of the spur gear system are investigated. The design parameters are listed in Table 1. For comparing convenience, the investigations on the coupling effects are performed at the following operating speeds: (1) at $n_1$=800 rpm to represent low-speed dynamic conditions away from any resonance, (2) at $n_1$=1100 rpm near the second super-harmonic resonance peak, (3) at $n_1$=1860 rpm near the first super-harmonic resonance peak, (4) at $n_1$=2200 rpm to represent a higher speed off-resonance condition, (5) at $n_1$=3720 rpm near the primary resonance peak.

### *4.1. Effects of surface wear on mesh stiffness and static transmission error*

The effects of surface wear on the mesh stiffness of the example system are demonstrated in Fig.4. As shown in Fig. 4(a), the spur gear pair experiences 1.74 mesh cycles from the starting point to the ending piont. In general, the mesh

stiffness decreases with the increment of surface wear depths during the double contact zone. The influneces of surface wear on the mesh stiffness are however, quite complicated during the transition region from double conatce zone to single contact zone. This may be explained by the reason that the surface wear alters the contact condition of the gear pair.

Fig. 4(b) demonstrates the effects of maximum wear depth on the mean value and the root-mean-square (rms) value as well as the first three harmonic amplitudes of the mesh stiffness of the example system. As can be clearly observed, the mean value of the mesh stiffness $k_{mm}$ decreases monotonously with the accumulation of wear depth. Meanwhile, the rms value and the first three harmonic amplitudes of the mesh stiffness almost monotonously increase with the accumulated surface wear. Compared to the first harmonic amplitude $k_1$ and the third harmonic amplitude $k_3$, variations of the rms value $k_{rms}$ and the second harmonic amplitude $k_2$ caused by the surface wear are quite noticable. The wear-caused variations of these harmonic components of mesh stiffness will aggravate the internal excitation of time-varying mesh stiffness, which in turn, degenerates the dynamics behaviors of the gear system.

The effects of surface wear on the STE of the example system are demonstrated in Fig. 5. As can be observed from Fig. 5(a), the STE decreases monotonously with the increment of wear depth during the majority of the mesh cycles. Similar to the variations of mesh stiffness, the influences of wear depth on the STE are complicated at the transition region of double contact zone to single contact zone. Fig. 5(b) shows that the influences of wear depth on the rms value $(STE)_{rms}$ and the second harmonic amplitude $(STE)_2$ are much more 'stronger' than those on $(STE)_1$ and $(STE)_3$. As one of the major internal excitation sources, the variations of STE caused by surface wear will also change the dynamic characteristics of the gear system.

Time-varying mesh stiffness excitation and gear transmission error excitation are the main contributors to gear vibration and noise. Accordingly, the influences of surface wear on mesh stiffness and transmission error must be considered in the problem of gear vibration and noise.

*4.2. Effect of surface wear on dynamic characteristics*

By considering the internal exciatation contributions from the surface wear, the dynamnic behaviors of the example system are predicted with the nonlinear dynamic model. In order to evaluate the effects of surface wear on the system dynamics, the dynamic mesh force $F_m$ of the spur gear pair without surface wear is taken as the baseline at each operational speed condition mentioned above.

As shown in Fig. 6, $F_m$ fluctuates within a certain range during the mesh cycles. Compared with high speed or resonant operational conditions, the fluctuation of $F_m$ is smaller when the system works at lower speed or non-resonant situation. For low or medium speed operations (the first four operational conditions), $F_m$ is always a non-zero value, demonstrating that there barely exists tooth separations. On the contrary, when the system works at high speed of $n_1$=3720 rpm, the dynamic mesh force $F_m$ becomes zero for about 44% of the time domain caused by tooth separations. A typical circumstance occurs when the system works at the condition of $n_1$=1860 rpm in that $F_m$ almost turns to be zero at one position during a whole mesh period. It implies that the gear system reaches the 'threshold' of tooth separations at this time interval.

By comparing the above dynamic mesh force $F_m$ with the results in the study of Ding and Kahraman [16], we can find that the steady-state dynamic responses obtained from the present model and Ding's model are slightly different. For example, the value of $F_m$ reaches zero twice during a mesh period when the sytem works at $n_1$=1860 rpm and $F_m$ becomes zero for about 40% of time domain when the operating speed is $n_1$=3720 rpm in Ding's study [16]. The differences in dynamic responses are aroused by the translational deflections that are considered in our model. With the consideration for additional translational motions of the gears, the prediction accuracy for nonlinear dynamic behaviors of the system can be improved.

Fig.7 shows the time histories of $F_m$ at the five operation speeds after the gear system runs for 3, 20, 40 and 100 million cycles of wear. By comparing Fig. 7 with Fig. 6, the effects of surface wear on dynamic responses of the example system can be revealed.

In general, the peak-to-peak amplitude of $F_m$ first decreases and then increases with the increment of wear cycles. Meanwhile, the tooth separations can be observed after some wear cycles. However, the effects of surface wear on $F_m$

are not exactly the same for different operational conditions. To be specific, it can be observed from Fig. 7(a) that the peak-to-peak amplitude of $F_m$ at $n_1$=800 rpm firstly decreases and then increases after 20 million wear cycles; meanwhile, obvious tooth separations can be observed after 100 million wear cycles though the separation duration in each mesh cycle is very short.

Fig. 7(b) shows that the peak-to-peak amplitude of $F_m$ at $n_1$=1100 rpm firstly decreases with wear and then increases after 40 million wear cycles; meanwhile, obvious tooth separations occur at 100 million wear cycles though the separation duration in each mesh cycles is also very short.

Similarly, the peak-to-peak amplitude of $F_m$ at $n_1$=1860 rpm decreases slightly and then increases at the tuning point of 20 million mesh cycles. The tooth separations take place after 40 million wear cycles and become obvious after 100 million wear cycles. The peak-to-peak amplitude of $F_m$ at $n_1$=2200 rpm decreases slightly before 20 million wear cycles and then increases dramatically after 100 million wear cycles. Meanwhile, the tooth separations last for about 44% of one mesh cycle after 100 million wear cycles.

It is very interesting that the tooth separations occur in the unworn gear pair worked at $n_1$=3720 rpm (as observed in Fig. 6) are eliminated after 3 million wear cycles and reappear after 100 million wear cycles as shown in Fig.7(e). Moreover, the peak-to-peak amplitude of $F_m$ increases monotonously with wear cycles, which is different from those of low and medium operation speeds. In can be roughly concluded that the initial surface wear may contribute to the reduction of the dynamic mesh force amplitudes and also help to eliminate tooth separations of the gear pair when the system operates at a resonance peek. After some wear cycels, the accumualted wear amounts may increase the amplitudes of dynamic mesh force and arouse tooth separations again. The influences of surface wear on the nonlinear dynamic behavior are more outstanding when the gear system operated at a higher speed.

The effects of surface wear on equivalent load of the spur gear system are further investigated and depicted in Fig. 8. For a spur gear system without worn surfaces, the equivalent load at primary resonance peak ($n_1$=3720 rpm) is much larger than those at the other speeds. However, situations may change after some wear cycles. For example, the equivalent load at an off-resonance speed of $n_1$=2220 rpm claims the highest value after the gear system runs for 100 million wear cycles.

Similar to the variations of dynamic mesh forces, the equivalent load firstly decreases and then increases with the increment of wear cycles at the five speeds.

To address the influences of surface wear more clearly, this paper defines the dynamic factor of the gear pair as DF=$(DMF)_{max}$/SMF, where $(DMF)_{max}$ is the maximum value of the dynamic mesh force in a mesh cycle and SMF is the static mesh force transmitted by the gear pair. The influences of surface wear on the dynamic factor are shown in Fig. 9.

As can be clearly observed, DF achieves the highest value at $n_1$=3720 rpm for a gear system without surface wear. This DF value drops dramatically after 3 million wear cycles and then increases monotonously with the wear accumulations. Similar trends can also be found in the other four operation conditions except that the DF values are smaller and the turning points of wear cycles are different. Once again, it can be found that the influences of surface wear on DF become more obvious when the gear system working at high speed ranges. Also, it can be concluded that accumulated wear depth may aggravate the system dynamic behaviors.

The following will explore the effects of surface wear on DTE of the spur gear pair. The simulation results are shown in Fig. 10.

As can be observed from Fig. 10, the root-mean-square value of the dynamic transmission error $(DTE)_{rms}$ decreases with mild wear of the gear surfaces and then increases with the accumulation of surface wear when the system works at low operating speed of $n_1$=800 rpm and high operating speed of $n_1$=3720 rpm. On the contrary, $(DTE)_{rms}$ decreases with the wear cycles at the operating speeds of $n_1$=1100 rpm, $n_1$=1860 rpm and $n_1$=2200 rpm.

At low-speed conditions away from any resonance ($n_1$=800 rpm), the third harmonic of DTE $(DTE)_3$ is higher than the first harmonic of DTE $(DTE)_1$ and the second harmonic of DTE $(DTE)_2$, making $(DTE)_{rms}$ is dominated by $(DTE)_3$. Surface wear is capable of increasing $(DTE)_3$ resulting in an increase in $(DTE)_{rms}$ beyond 20 million wear cycles. Near the superharmonic resonances ($n_1$=1100 rpm and $n_1$=1860 rpm), $(DTE)_2$ is higher and dominates $(DTE)_{rms}$. $(DTE)_{rms}$ decreases with wear cycles duo to the reduction of $(DTE)_2$ beyond 40 million cycles. At higher speed off-resonance conditions ($n_1$=2200 rpm), $(DTE)_3$ is very small compared to $(DTE)_1$ and $(DTE)_2$. $(DTE)_{rms}$ is primarily impacted by $(DTE)_1$ and $(DTE)_2$. When the operating speed approaches the primary resonance peak ($n_1$=3720 rpm), $(DTE)_2$ and $(DTE)_3$ are smaller

than $(DTE)_1$ and as a result $(DTE)_{rms}$ is dominated by $(DTE)_1$. The first three harmonic amplitudes of DTE increase with wear significantly beyond 40 million cycles, making $(DTE)_{rms}$ turn to be higher.

Fig. 11 shows the effects of surface wear on the period of steady dynamic response of the example system.

As can be seen from Fig. 11, the periods of steady dynamic response retain the same after different wear cycles when the gear system operates at the other four speeds except $n_1$=3720 rpm. The period-four, period-three, period-two and period-eight responses are successively observed in dynamic analyses when the wear cycles increase from 0 to 100 million.

*4.3. Effect of gear dynamics on surface wear*

In order to study the effect of gear dynamics on surface wear, the static wear behaviors are adopted as a baseline for comparisons. The surface wear distributions of the pinion after different wear cycles under static load conditions are depicted in Fig. 12.

Fig. 13 indicates that during the early stages of wear, the influence of operational conditions on the maximum wear depth is quite trivial. The gaps of accumulated wear amounts between the five operational conditions and the static condition are very small. However, the accumulated wear depths change significantly with the operational speed when wear cycles exceed a range. The maximum wear depths at the four operation speeds (except for $n_1$=3720 rpm) are larger than that of the static condition after the same wear cycles. On the contrary, the maximum wear depth at the primary reasonant speed of $n_1$=3720 rpm is smaller than that of the static condition. Besides, the maximum wear depth accumulated at $n_1$=1100 rpm is the largest and the maximum wear depth at $n_1$=3720 rpm is the smallest. However, there exists no simple linear trend between the maximum wear depth and the operating speed. For example, the maximum wear depths at $n_1$=1860 rpm and $n_1$=2200 rpm are smaller than those at $n_1$=1100 rpm. The reason may lie in that the accumulated wear depth is affected by both the contact pressures and the wear coefficient. And the contact pressures are related to the mesh forces, which changes with the system's operating speed. The wear coefficient decreases when the operating speed increases [16]. When the gear syetem operates at $n_1$=1100 rpm, the equivalent load and the wear

coefficient are larger than those at other speeds, thus leads to the largest wear depth value at this operational condition. While at the primary resonance peak ($n_1$=3720 rpm), duo to the tooth separations, the contact chances of engaged mating surfaces are reduced to slow the accumulation of surface wear. To summerize, the wear depth is the largest when the example system operates near the second super-harmonic resonance peak while achives the smallest value near the primary resonance peak. The wear depth near a low-speed off-resonance condition is significantly smaller than those near the second super-harmonic resonance peak and the first super-harmonic resonance peak. The wear depth value near a higher speed off-resonance condition is larger than those near a low-speed off-resonance condition.

## 5. Conclusions

A dynamic wear prediction methodology is proposed by combining a translational-rotational-coupled nonlinear dynamic model with a quasi-static wear model to investigate the coupling effects between surface wear and dynamic behaviors in a spur gear system. Based on the analyses carried out in this study, the following conclusions can be drawn:

(1) The accumulated surface wear alters the mesh stiffness and the transmission error of the gear pair, thus affects the dynamic characteristic of the gear system significantly.

(2) The initial surface wear contributes to reduce the amplitudes of dynamic response and eliminate tooth separations of the gear pair operated at a resonance peek. However, additional wear amounts may aggravate the system vibration characteristics and cause tooth separations.

(3) The effects of surface wear on period of steady dynamic response are negligible except for the primary resonance peak.

(4) To improve the wear prediction accuracy, the translational deflections in the gear system must be included.

(5) During the mild wear stages, the effect of operational condition on surface wear is very weak. However, the wear depths are affected by the operating speed noticeably after some wear cycles.

(6) The wear depth values are the largest when the gear system operates near the second super-harmonic resonance peak while achieve the smallest when operates near the primary resonance peak.

Our future work focuses on the effect of load, tooth modification, bearing stiffness and misalignment on both system dynamics and surface wear.

**Acknowledgements**

This work is jointly sponsored by National Natural Science Foundation of China (Grant No. 51375013, 50905122, 51405003) and Anhui Provincial Natural Science Foundation (Grant No. 1208085ME64).

**References**


1. Kahraman A, Singh R. Non-linear dynamics of a spur gear pair. Journal of Sound and Vibration 1990;142(1):49-75. doi:10.1016/0022-460X(90)90582-K

2. Kahraman A, Singh R. Interactions between time-varying mesh stiffness and clearance non-linearities in a geared system. Journal of Sound and Vibration 1991;146(1):135-56. doi:10.1016/0022-460X(91)90527-Q

3. Parker RG, Vijayakar SM, Imajo T. Non-linear dynamic response of a spur gear pair: modelling and experimental comparisons. Journal of Sound and Vibration 2000;237(3):435-55. doi:10.1006/jsvi.2000.3067

4. Shen Y, Yang S, Liu X. Nonlinear dynamics of a spur gear pair with time-varying stiffness and backlash based on incremental harmonic balance method. Journal of Mechanical Sciences 2006;48:1256-63. doi:10.1016/j.ijmecsci.2006.06.003

5. Li S, Kahraman A. A tribo-dynamic model of a spur gear pair. Journal of Sound and Vibration 2013;332(20):4963-78. doi:10.1016/j.jsv.2013.04.022

6. Farshidianfar A, Saghafi A. Identification and control of chaos in nonlinear gear dynamic systems using Melnikov analysis. Physics Letters A 2014;378:3457-63. doi:10.1016/j.physleta.2014.09.060

7. Atanasovska I. The mathematical phenomenological mapping in non-linear dynamics of spur gear pair and radial ball bearing due to the variable stiffness. International Journal of Non-Linear Mechanics 2015;73:114-20. doi:10.1016/j.ijnonlinmec.2014.11.015

8. Choy FK, Polyshchuk V, Zakrajsek JJ, et al. Analysis of the effects of surface pitting and wear on the vibration of a gear transmission system. Tribology International 1996;29(1):77-83. doi:10.1016/0301-679X(95)00037-5

9. Wojnarowski J, Onishchenko V. Tooth wear effects on spur gear dynamics. Mechanism and Machine Theory 2003;38:161-78. doi:10.1016/S0094-114X(02)00091-5

10. Yesilyurt I, Gu F, Ball AD. Gear tooth stiffness reduction measurement using modal analysis and its use in wear fault severity assessment of spur gears. NDT&E International 2003;36:357-72. doi:10.1016/S0963-8695(03)00011-2

11. Kuang JH, Lin AD. The effect of tooth wear on the vibration spectrum of a spur gear pair. Journal of vibration and acoustics 2001;123(3):311-7. doi:10.1115/1.1379371

12. Lin AD, Kuang JH. Dynamic interaction between contact loads and tooth wear of engaged plastic gear pairs. International Journal

of Mechanical Sciences 2008;50(2):205-13. doi:10.1016/j.ijmecsci.2007.07.002

13. Yuksel C, Kahraman A. Dynamic tooth loads of planetary gear sets having tooth profile wear. Mechanism and Machine Theory 2004;39(7):695-715. doi:10.1016/j.mechmachtheory.2004.03.001

14. Osman T, Velex Ph. Static and dynamic simulations of mild abrasive wear in wide-faced solid spur and helical gears. Mechanism and Machine Theory 2010;45(6):911-24. doi:10.1016/j.mechmachtheory.2010.01.003

15. Wu S, Cheng HS. Sliding wear calculation in spur gears. Journal of Tribology 1993;115(3):493-500. doi:10.1115/1.2921665

16. Ding H, Kahraman A. Interactions between nonlinear spur gear dynamics and surface wear. Journal of Sound and Vibration 2007;307(3):662-79. doi:10.1016/j.jsv.2007.06.030

17. Kahraman A, Ding H. A methodology to predict surface wear of planetary gears under dynamic conditions. Mechanics Based Design of Structures and Machines 2010;38(4):493-515. doi:10.1080/15397734.2010.501312

18. Põdra P, Andersson S. Wear simulation with the Winkler surface model. Wear 1997;207(1):79-85. doi:10.1016/S0043-1648(96)07468-6

19. Flodin A, Andersson S. Simulation of mild wear in spur gears. Wear 1997;207(1):16-23. doi:10.1016/S0043-1648(96)07467-4

20. Flodin A, Andersson S. Simulation of mild wear in helical gears. Wear 2000;241(2):123-8. doi:10.1016/S0043-1648(00)00384-7

21. Flodin A, Andersson S. A simplified model for wear prediction in helical gears. Wear 2001;249(3):285-92. doi:10.1016/S0043-1648(01)00556-7

22. Brauer J, Andersson S. Simulation of wear in gears with flank interference-a mixed FE and analytical approach. Wear 2003;254(11):1216-32. doi:10.1016/S0043-1648(03)00338-7

23. Bajpai P, Kahraman A, Anderson NE. A surface wear prediction methodology for parallel-axis gear pairs. Journal of Tribology 2004;126(3):597-605. doi:10.1115/1.1691433

24. Kahraman A, Bajpai P, Anderson NE. Influence of tooth profile deviations on helical gear wear. Journal of Mechanical Design 2005;127(4):656-63. doi:10.1115/1.1899688

25. Karpat F, Ekwaro-Osire S. Influence of tip relief modification on the wear of spur gears with asymmetric teeth. Tribology Transactions 2008;51(5):581-8. doi:10.1080/10402000802011703

26. Dhanasekaran S, Gnanamoorthy R. Gear tooth wear in sintered spur gears under dry running conditions. Wear 2008;265(1):81-7. doi:10.1016/j.wear.2007.08.025

27. Hegadekatte V, Hilgert J, Kraft O, Huber N. Multi time scale simulations for wear prediction in micro-gears. Wear 2010;268(1):316-24. doi:10.1016/j.wear.2009.08.017

28. Mao K, Li W, Hooke CJ, Walton D. Polymer gear surface thermal wear and its performance prediction. Tribology International 2010;43:433-9. doi:10.1016/j.triboint.2009.07.006

29. Amarnath M, Praveen Krishna IR. Detection and diagnosis of surface wear failure in a spur geared system using EEMD based vibration signal analysis. Tribology International 2013;61:224-34. doi:10.1016/j.triboint.2013.01.001

30. Tunalioğlu MŞ, Tuç B. Theoretical and experimental investigation of wear in internal gears. Wear 2014;309(1):208-15. doi:10.1016/j.wear.2013.11.016

31. Fernandes C, Battez AH, González R, et al. Torque loss and wear of FZG gears lubricated with wind turbine gear oils using an ionic liquid as additive. Tribology International 2015;90:306-14. doi:10.1016/j.triboint.2015.04.037

32. Zhang J, Liu XZ. Effects of misalignment on surface wear of spur gears. Proceedings of the Institution of Mechanical Engineers, Part J: Journal of Engineering Tribology 2015;229(9):1145-58. doi:10.1177/1350650115574732

33. Kahraman A, Kharazi A, Umrani M. A deformable body dynamic analysis of planetary gears with thin rims. Journal of Sound and Vibration 2003;262(3):752-68. doi:10.1016/S0022-460X(03)00122-6

34. Feng ZP, Zuo MJ. Fault diagnosis of planetary gearboxes via torsional vibration signal analysis. Mechanical Systems and Signal Processing 2013;36:401-21. doi:10.1016/j.ymssp.2012.11.004

35. Inalpolat M, Kahraman A. A dynamic model to predict modulation sidebands of a planetary gear set having manufacturing errors. Journal of Sound & Vibration 2010;329(4):371-93. doi:10.1016/j.jsv.2009.09.022

36. Li XM, Sosa M, Andersson M, Olofsson Ulf. A study of the efficiency of spur gears made of powder metallurgy materials–ground versus super-finished surfaces. Tribology International 2016;95:211-20. doi:10.1016/j.triboint.2015.11.021

37. Miner MA. Cumulative damage in fatigue. Journal of Applied Mechanics 1945;12(3):159-62.

38. American Gear Manufacturers Association. ANSI/AGMA/AWEA 6006-A03 Standard for design and specification of gearboxes for

wind turbines. United states of American: American National Standard Institute 2004;79-81.

# Highlights

1. A combined model based dynamic wear prediction methodology for a spur gear system is proposed.
2. The proposed dynamic model takes into account the translational deflections in the gear system to improve the wear prediction accuracy.
3. The coupling effects between surface wear and dynamic behaviors in a spur gear system are investigated quantitively.

Graphical abstract

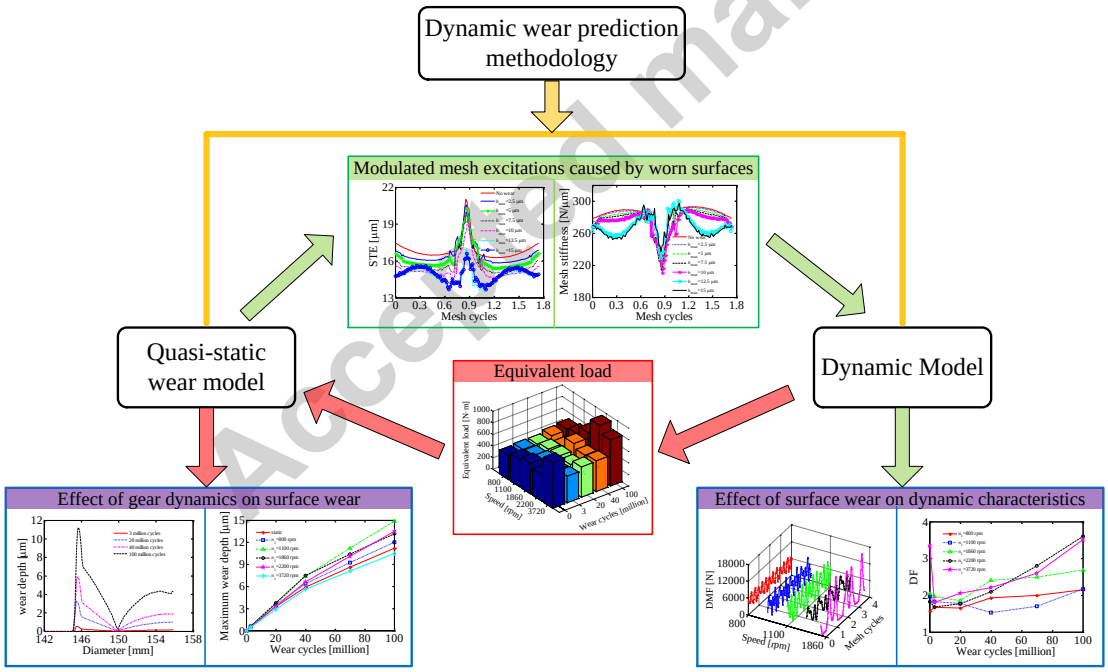


## List of Figure Captions

**Fig. 1** Nonlinear dynamic model for a spur gear system

**Fig. 2** Computational methodology of gear wear

**Fig. 3** Computational methodology of dynamic wear

**Fig. 4** Variation of mesh stiffness with maximum wear depth

**Fig. 5** Variation of static transmission error with maximum wear depth

**Fig. 6** Time histories of $F_m$ without wear at five operational conditions

**Fig. 7** Time histories of $F_m$ after various wear cycles at (a) $n_1$=800 rpm, (b) $n_1$=1100 rpm, (c) $n_1$=1860 rpm, (d) $n_1$=2200 rpm, (e) $n_1$=3720 rpm

**Fig. 8** Variations of equivalent load with wear cycles

**Fig. 9** Variations of dynamic factor with wear cycles

**Fig. 10** Variation of dynamic transmission error with wear cycles at (a) $n_1$=800 rpm, (b) $n_1$=1100 rpm, (c) $n_1$=1860 rpm, (d) $n_1$=2200 rpm, (e) $n_1$=3720 rpm. (–⁎–) $(DTE)_{rms}$, (..□..) $(DTE)_1$, (–·Δ·–) $(DTE)_2$, (--○--) $(DTE)_3$

**Fig. 11** Phase plane plots of steady dynamic response $u$ after various wear cycles at (a) $n_1$=800 rpm, (b) $n_1$=1100 rpm, (c) $n_1$=1860 rpm, (d) $n_1$=2200 rpm, (e) $n_1$=3720 rpm

**Fig. 12** Wear distributions of the pinion after various wear cycles at static operation condition

**Fig. 13** Variation of maximum wear depth with respect to wear cycles at different operational conditions

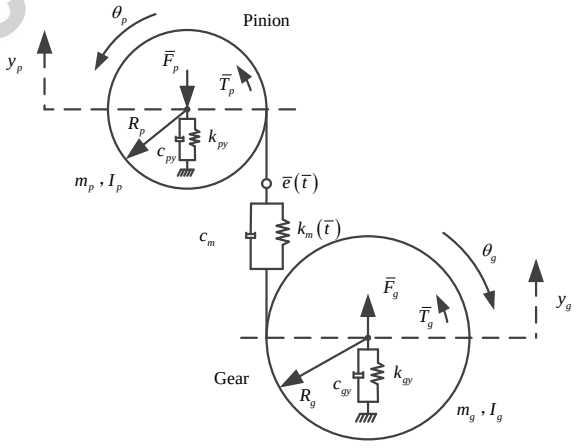


**Fig. 1.** Nonlinear dynamic model for a spur gear system.

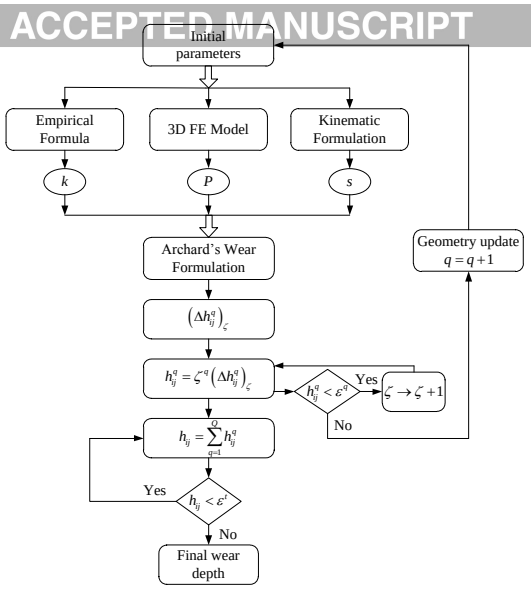


**Fig. 2.** Computational methodology of gear wear.

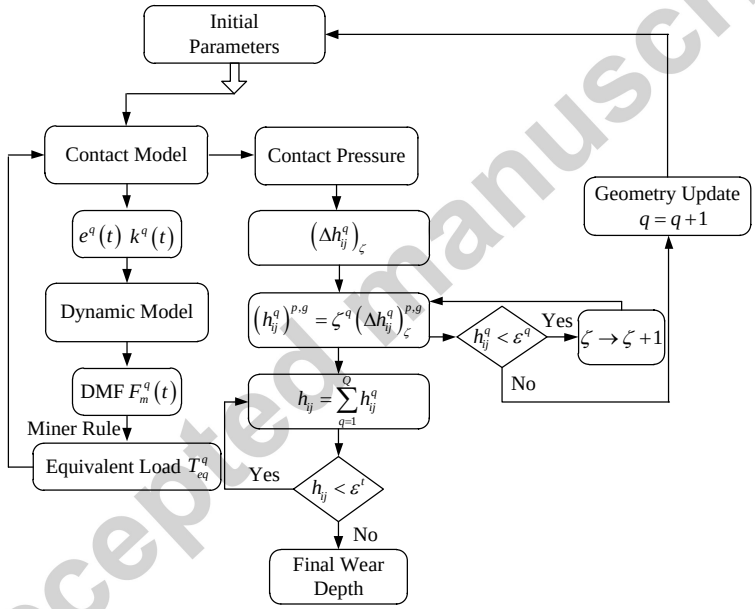


**Fig. 3.** Computational methodology of dynamic wear.

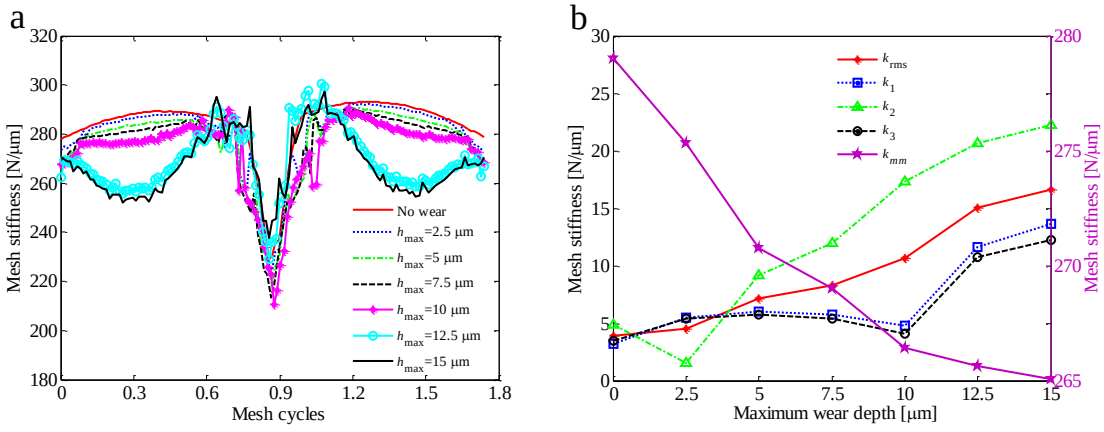

**Fig. 4.** Variation of mesh stiffness with maximum wear depth.

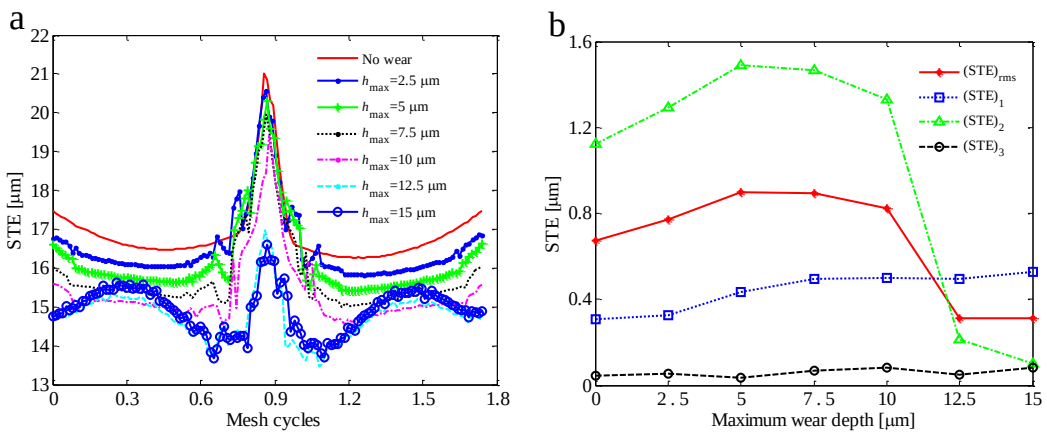


**Fig. 5.** Variation of static transmission error with maximum wear depth.

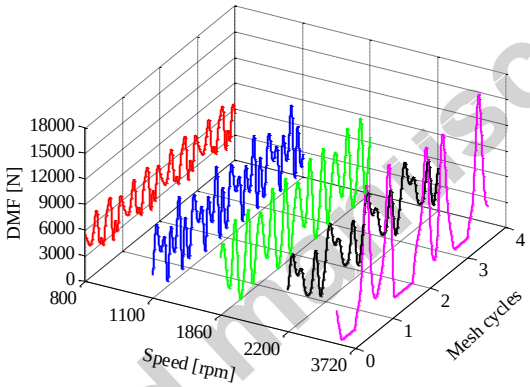


**Fig. 6.** Time histories of $F_m$ without wear at five operational conditions.

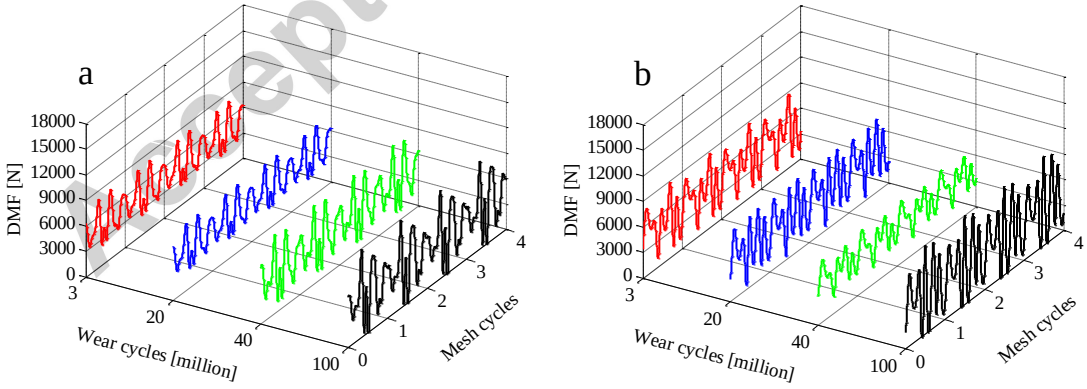

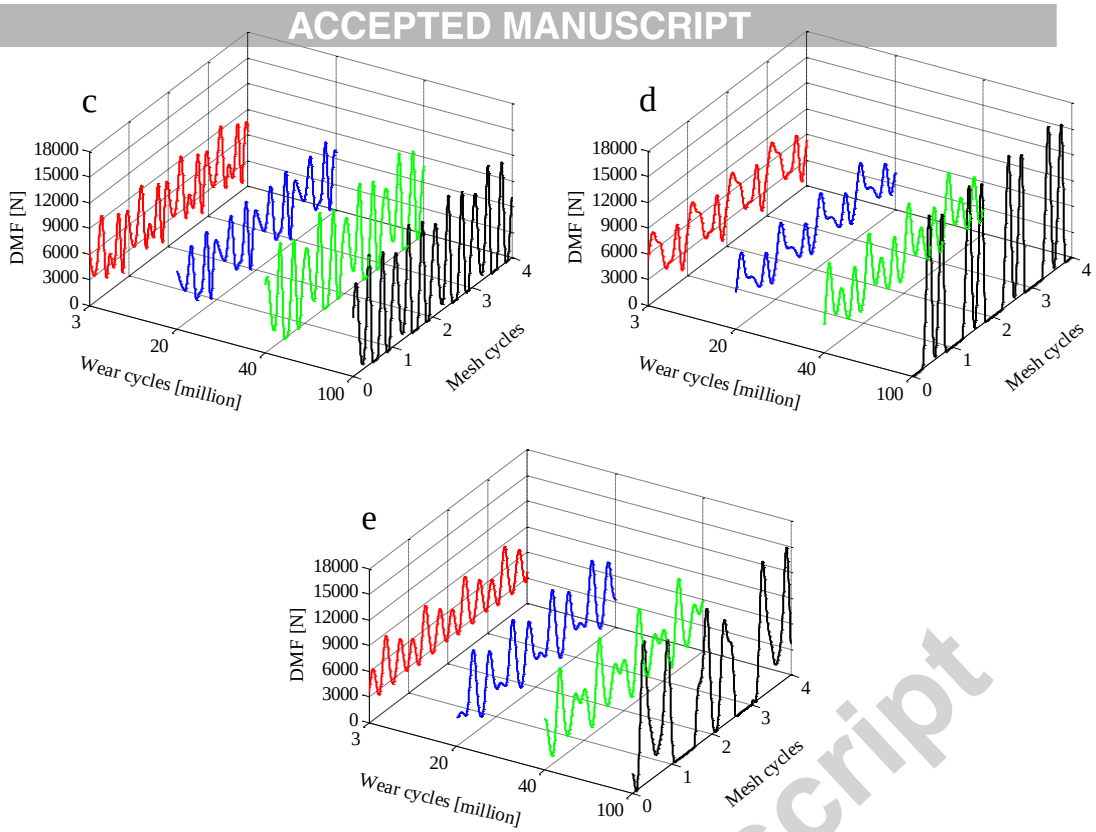


**Fig. 7.** Time histories of $F_m$ after various wear cycles at (a) $n_1$=800 rpm, (b) $n_1$=1100 rpm, (c) $n_1$=1860 rpm, (d) $n_1$=2200 rpm, (e) $n_1$=3720 rpm.

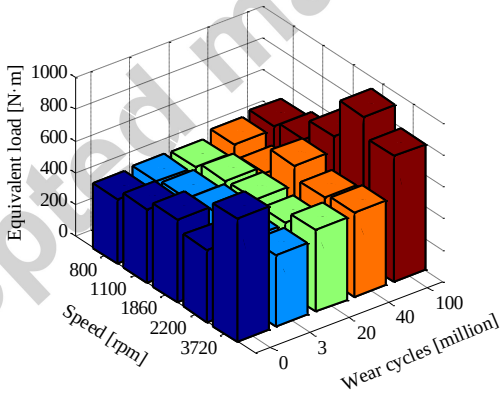


**Fig. 8.** Variations of equivalent load with wear cycles.

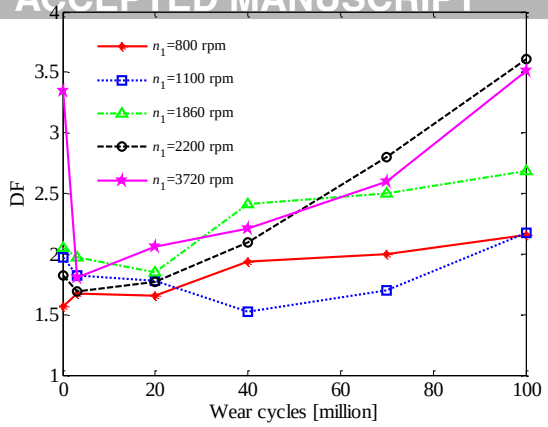


**Fig. 9.** Variations of dynamic factor with wear cycles.

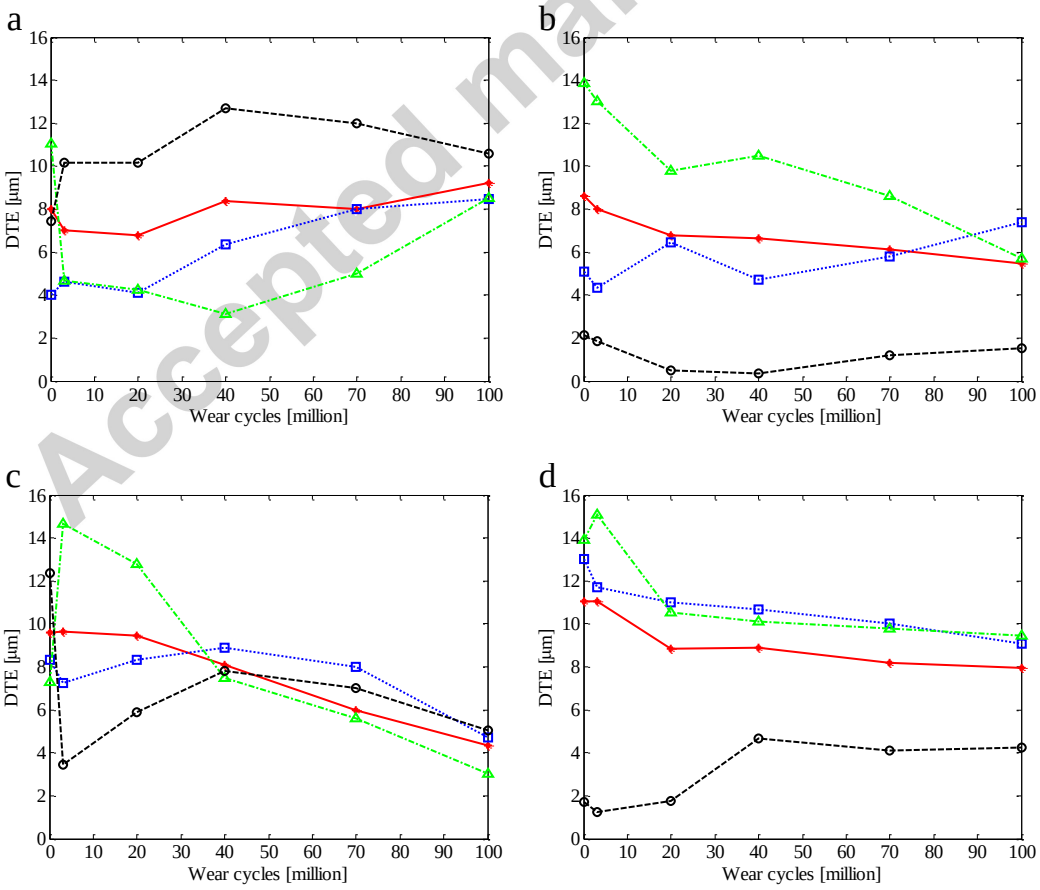

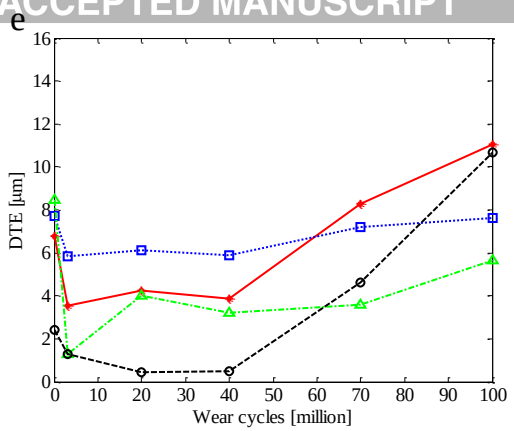


**Fig. 10.** Variation of dynamic transmission error with wear cycles at (a) $n_1$=800 rpm, (b) $n_1$=1100 rpm, (c) $n_1$=1860 rpm, (d) $n_1$=2200 rpm, (e) $n_1$=3720 rpm. (–⁎–) $(DTE)_{rms}$, (..□..) $(DTE)_1$, (–·△·–) $(DTE)_2$, (--○--) $(DTE)_3$.

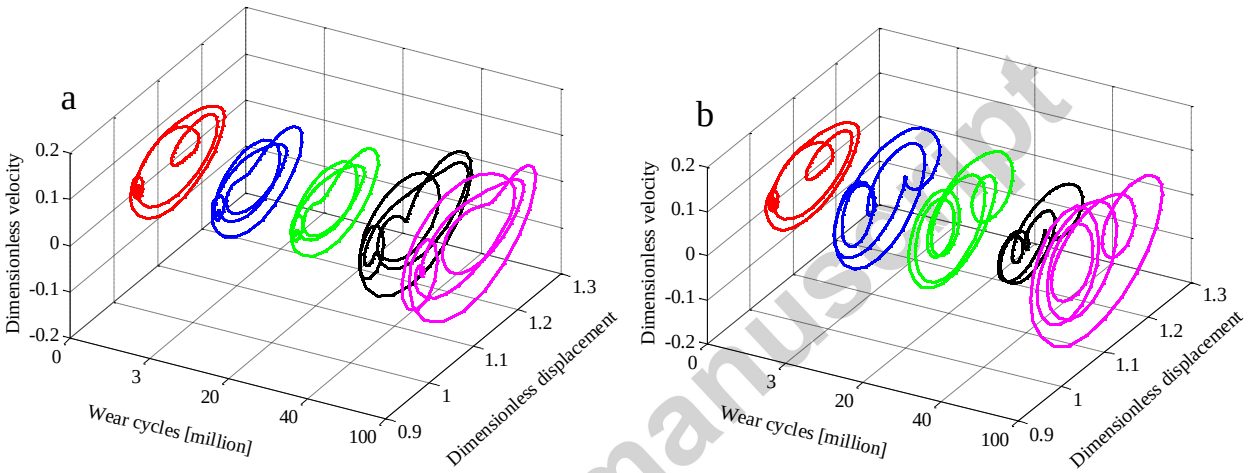

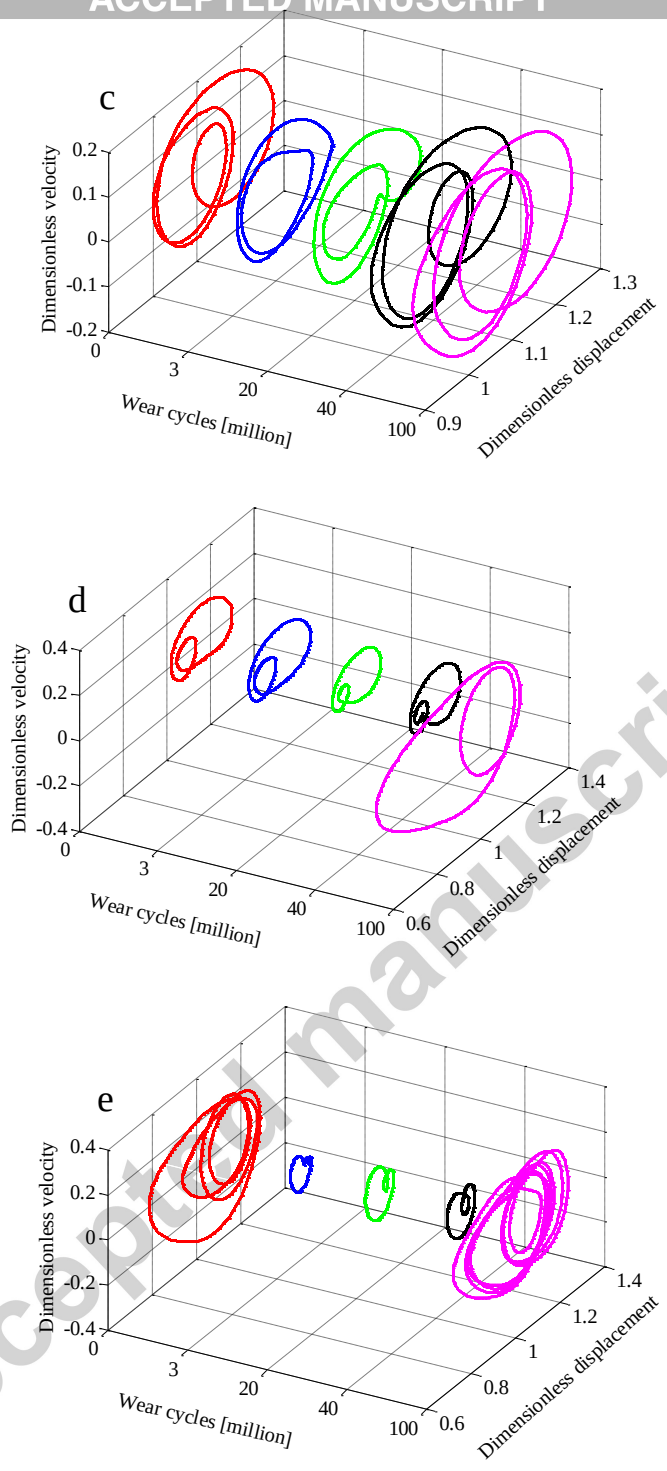




**Fig. 11.** Phase plane plots of steady dynamic response $u$ after various wear cycles at (a) $n_1$=800 rpm, (b) $n_1$=1100 rpm, (c) $n_1$=1860 rpm, (d) $n_1$=2200 rpm, (e) $n_1$=3720 rpm.

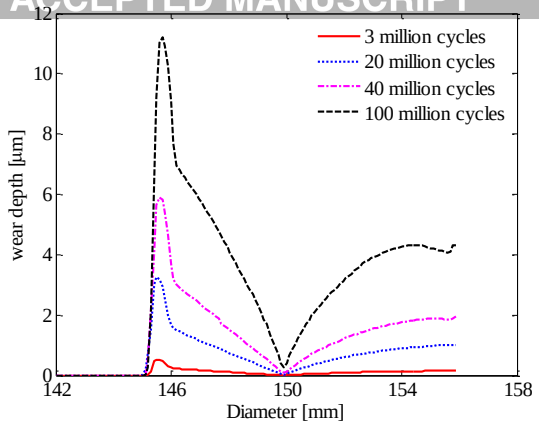


**Fig. 12.** Wear distributions of the pinion after various wear cycles at static operation conditon.

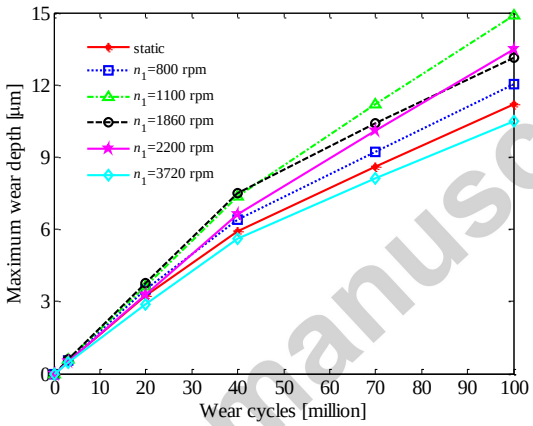


**Fig. 13.** Variation of maximum wear depth with respect to wear cycles at different operational conditions.



## List of Tables



**Table 1** Parameters of the example system.

| Parameter Nomenclatures | Pinion *p* | Gear *g* | Parameter Nomenclatures | Pinion *p* | Gear *g* |
|---|---|---|---|---|---|
| Number of tooth *z* | 50 | 50 | Module $m_n$/mm | 3.0 | 3.0 |
| Pressure angle $\alpha_n$/(°) | 20 | 20 | Tooth width *B*/mm | 20 | 20 |
| Pitch diameter $d_w$/mm | 150 | 150 | Base diameter $d_b$/mm | 140.95 | 140.95 |
| Addendum diameter $d_a$/mm | 156 | 156 | Dedendum diameter $d_f$/mm | 140 | 140 |
| Material | 42CrMo | 42CrMo | Density $\rho$/(kg·m$^{-3}$) | 7830 | 7830 |
| Young's modulus *E*/GPa | 206 | 206 | Poisson's ratio $\upsilon$ | 0.3 | 0.3 |

| | | | | | |
|---|---|---|---|---|---|
| Mass $m$/kg | 2.8 | 2.8 | Moment of inertia $I$/(kg·mm$^2$) | 7300 | 7300 |
| Bearing stiffness $k_y$/(N/μm) | 1150 | 1150 | Bearing damping $c$/(Ns/m) | 5360 | 5360 |
| Roughness $R_a$/μm | 0.3 | 0.3 | ISO precision grade | 5 | 5 |
| Meshing damping $c_m$/(N·s/m) | 1000 | | | | |
| Input torque $T_p$/(N·m) | 340 | | | | |
| Center distance $a$/mm | 150 | | | | |